ChemComm

COMMUNICATION

View Article Online
View Journal | View Issue

Cite this: *Chem. Commun.*, 2025, **61**, 5778

Received 5th February 2025,
Accepted 14th March 2025

DOI: 10.1039/d5cc00646e

rsc.li/chemcomm

A strong H-bond between a cysteine and the catalytic center of a [NiFe]-hydrogenase†

Chara Karafoulidi-Retsou, Sagie Katz, Stefan Frielingsdorf, Oliver Lenz, Ingo Zebger * and Giorgio Caserta *

Infrared spectroscopy at cryogenic temperatures was used to monitor protonation changes on an H^+-accepting, nickel-coordinating active site cysteine of the H_2/H^+-cycling membrane-bound [NiFe]-hydrogenase from *Cupriavidus necator*. Surprisingly, we identified another cysteine in the outer coordination sphere forming a strong H-bond with a cysteine thiolate coordinating both nickel and iron of the catalytic center.

[NiFe]-hydrogenases catalyze the reversible cleavage of dihydrogen into protons and electrons at a bioinorganic heterobimetallic [NiFe] center. This active site is anchored to the large catalytic subunit of the hydrogenase heterodimeric functional unit, known as the hydrogenase module, by four cysteine residues coordinating the nickel ion. Two of these cysteines act as bridging ligands between the Ni and Fe ions. The Fe is further ligated by two cyanides (CN^-) and one carbonyl (CO) ligand (Fig. 1a).[1,2] During H_2 activation, protons are transferred to nearby H^+-accepting residues, while electrons are shuttled to redox partners *via* an array of Fe–S clusters. The catalytic cycle involves several intermediates (Fig. 1b), whose detailed structures have not yet been fully elucidated, despite ongoing efforts of various research groups.[3–5] Vibrational spectroscopic techniques, in particular infrared (IR) spectroscopy, are valuable tools in hydrogenase research.[6–8] The power of IR spectroscopy arises from the presence of the CO and CN^- ligands (Fig. 1a),[4,9] which absorb in a frequency regime unaffected by protein or solvent bands, and thus, represent valuable marker bands that react sensitively to redox, acid–base and structural changes taking place at or near the [NiFe] site.[3] Recently, the applicability of IR spectroscopy on hydrogenases has been further expanded, enabling the identification of individual amino acids as both coordinating and localized in the vicinity of the active site (*e.g.*, within H-bonding distance).[10–12] In 2019, the Hirota group was the first to use IR difference spectroscopy at cryogenic temperatures to detect the S–H stretching vibration of the so-called Ni_a-L intermediate (Fig. 1b) in the [NiFe]-hydrogenase from *Desulfovibrio vulgaris* Miyazaki F (*Dv*MF).[11] Such absorptions are difficult to discern due to their inherently low molar absorption coefficients. The IR data for *Dv*MF hydrogenase were interpreted as transient protonation of a Ni-coordinating cysteine residue that acts as a H^+ acceptor in the photolysis of the bridging hydride of the Ni_a-C intermediate (Fig. 1b).[13] Recently, we have further extended the mechanistic knowledge of the Ni_a-C → Ni_a-L transformation.[14] For the O_2-tolerant regulatory hydrogenase from *Cupriavidus necator* (*Cn*RH), we observed that this transformation initially forms the metastable Ni_a-L1 species, which then rapidly converts into the well-characterized Ni_a-L2 species. Importantly, in both Ni_a-L intermediates, a Ni-bound cysteine thiolate is protonated and the Ni_a-C → Ni_a-L1 → Ni_a-L2 conversions were accompanied by subtle structural rearrangements in the 2nd coordination sphere of the active site. Although a protonated cysteine is now generally accepted as an integral part of the Ni_a-L intermediate, the corresponding low-temperature IR absorptions have only been detected for *Cn*RH and *Dv*MF hydrogenase, while the IR spectroscopic analysis of the O_2-tolerant [NiFe]-hydrogenase 1 from *Escherichia coli* (*Ec*Hyd1) did not reveal any change in the protonation state of the corresponding thiolate side chain.[15] Here, we intended to verify the protonation of the corresponding Ni-bound cysteine using the membrane-bound [NiFe]-hydrogenase from *C. necator* (*Cn*MBH), which is structurally and functionally closely related to *Ec*Hyd1. As-isolated oxidized *Cn*MBH resides predominantly in the Ni_r-B resting state with a hydroxy ligand in the bridging position of the active site.[16] In the corresponding IR spectrum, this intermediate is characterized by a stretching vibration of the CO ligand (ν_{CO}) at 1948 cm^{-1} and stretching vibrations of the CN^- ligands (ν_{CN}) at 2081 and 2098 cm^{-1} (Fig. S1, ESI†). After 30-min reduction with H_2 at pH 5.5 and 283 K, the corresponding IR spectrum shows predominantly signals of the Ni_a-C intermediate (Fig. S2, ESI†). In contrast, IR data recorded in a 280–210 K temperature window (Fig. 2a) show the presence of a

Institut für Chemie, Technische Universität Berlin, Straße des 17. Juni 135, 10623 Berlin, Germany. E-mail: ingo.zebger@tu-berlin.de, giorgio.caserta@tu-berlin.de

† Electronic supplementary information (ESI) available: Experimental procedures, supplementary figures, supplementary discussion, and supplementary references. See DOI: https://doi.org/10.1039/d5cc00646e

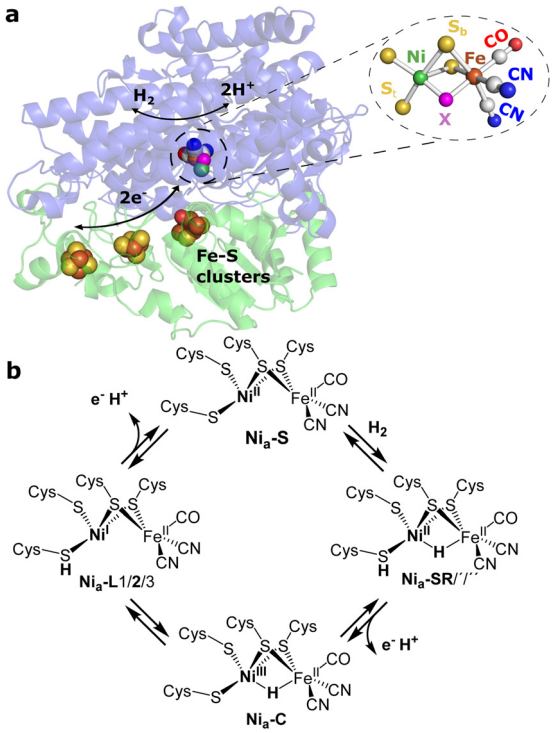

Fig. 1 Membrane-bound [NiFe]-hydrogenase from *Cupriavidus necator* (*Cn*MBH) and the consensus catalytic cycle of [NiFe]-hydrogenases. (a) Cartoon representation of *Cn*MBH (PDB: 3RGW (**https://www.rcsb.org/structure/3RGW**)),[25] consisting of the catalytic large subunit (blue) and the electron-transferring small subunit (green), harboring three Fe–S clusters. The NiFe cofactor and the coordinating cysteines are shown in ball and stick representation. Color code: Ni, green; Fe, brown; CO oxygen, red; CN^- nitrogen, blue; corresponding carbon atoms, grey; bridging (S_b) and terminal (S_t) cysteine thiolates, yellow; the vacant bridging position is indicated by an X (magenta) and can be occupied either by hydroxy or hydride ligands. (b) Schematic representation of the generally accepted catalytic cycle of [NiFe]-hydrogenases. Nickel is the redox-active metal and can adopt the oxidation states$^{1+/2+/3+}$, while the iron maintains an Fe^{2+} low-spin configuration throughout the catalytic cycle. The proposed catalytic cycle involves the intermediates Ni_a-S, Ni_a-SR, Ni_a-C and Ni_a-L. Among them, the Ni_a-SR and Ni_a-L each comprise three sub-forms,[4,13,14] whose structural differences are not fully understood.

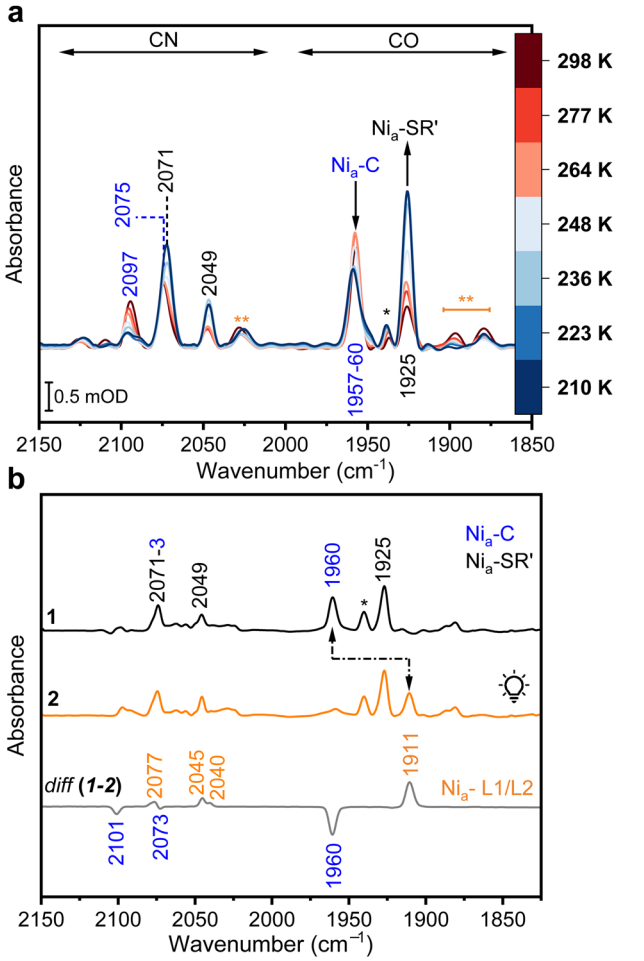

Fig. 2 IR spectroscopic characterization of *Cn*MBH. (a) IR absorbance spectra of H_2-reduced *Cn*MBH recorded between 210 and 298 K, indicating a temperature-dependent redox equilibrium between the Ni_a-C and the Ni_a-SR′ states. Characteristic CO/CN absorptions are labeled with the corresponding wavenumbers. (b) IR spectra of H_2-reduced *Cn*MBH at 95 K before (trace 1) and after light exposure (trace 2). Spectral changes are illustrated by black arrows and visualized in more detail by the related difference spectrum (trace diff (1–2)). The absorptions marked with a black asterisk are attributed to remnants of $Ni_a/_r$-S species (1936 cm^{-1}). ν_{CO} signals marked with two orange asterisks at 1895 and 1880 cm^{-1} are attributed to sub-stoichiometric amounts of Ni_a-L species enriched under dark conditions.

temperature-dependent equilibrium between the Ni_a-C (ν_{CO} at 1957 cm^{-1} and ν_{CN} at 2075 and 2097 cm^{-1}) and the Ni_a-SR′ (ν_{CO} at 1925 cm^{-1} and ν_{CN} at 2049 and 2071 cm^{-1}) state, the latter carrying one H^+ and one e^- more (Fig. 1b). The effect of temperature on the enrichment of certain hydrogenase intermediates has been observed previously,[17,18] and recently, temperature-dependent changes in the Ni_a-C ⇄ Ni_a-SR equilibrium have been reported for the NAD^+-reducing [NiFe]-hydrogenase from *Hydrogenophilus thermoluteolus* TH-1.[19] Our IR data of *Cn*MBH also included small amounts of Ni_a-L species even without light exposure (Fig. 2a and Fig. S2, ESI†), which is in agreement with the current view that Ni_a-L is a genuine intermediate of the catalytic cycle.[20–22] Upon illumination of the sample at 95 K (460 nm LED), Ni_a-C quantitatively converts to Ni_a-L species, characterized by a ν_{CO} at 1911 cm^{-1} (Fig. 2b, traces 1 and 2). The photoconversion is more clearly visible in the corresponding "light-minus-dark" difference spectrum (Fig. 2b, trace diff (1–2)). A closer inspection of the IR spectrum in the region of the ν_{CN} absorptions (2120–2020 cm^{-1}) reveals that two distinct Ni_a-L species are generated upon irradiation, which show almost overlapping CO absorptions at 1911 cm^{-1}, but distinct CN^- bands at 2040, 2045, and 2077 cm^{-1} (the latter partially overlapping with a ν_{CN} of Ni_a-C at 2073 cm^{-1}). The observed Ni_a-L species are comparable to the recently resolved Ni_a-L1 and Ni_a-L2 intermediates of *Cn*RH, where the two ν_{CO} bands are also close ($\Delta\nu_{CO} \approx 3$ cm^{-1}), while the corresponding (symmetric and antisymmetric) ν_{CN} showed larger differences (Fig. S3, ESI†).[14] Interestingly, for *Cn*MBH, two distinct bands at 2516 (negative, Ni_a-C) and 2523 cm^{-1} (positive, Ni_a-L) were observed in the S–H (ν_{SH}) region of the spectrum (Fig. 3a), indicating one or more protonated cysteines.[11,14,23] Both ν_{SH} absorptions appear in a spectral region of strongly H-bonded S–H side groups,[23] and

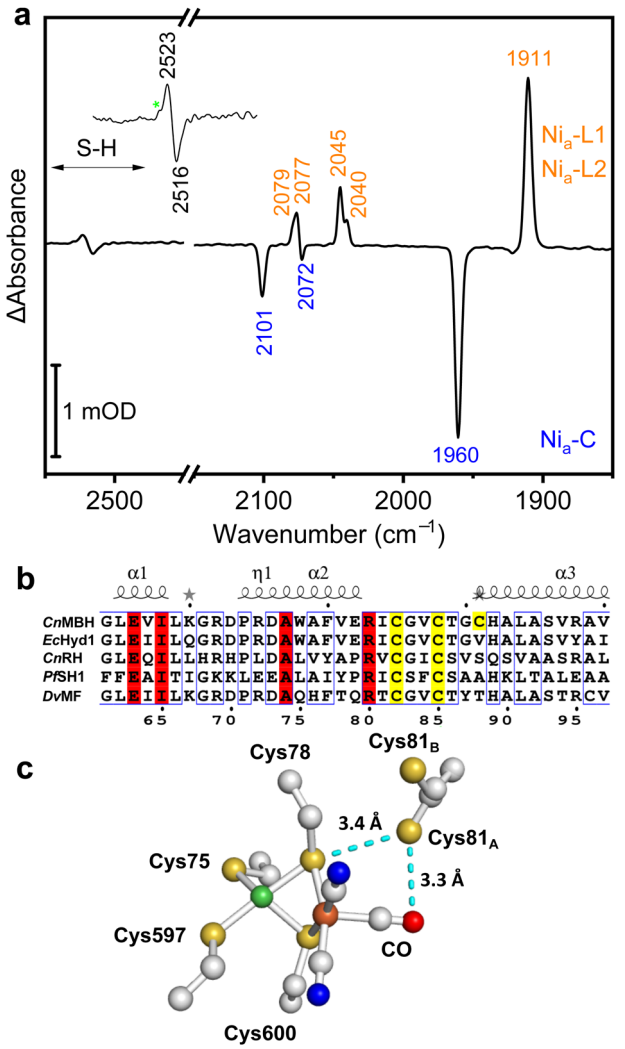

Fig. 3 An additional cysteine in *Cn*MBH is located near the NiFe site. (a) IR difference spectrum (light-minus-dark) of *Cn*MBH recorded at 95 K. Characteristic absorptions of CO, CN^- and SH are labeled with the corresponding wavenumbers. The inset in the upper left shows an enlargement of the SH bands. The minor absorption marked with an asterisk may result from the protonation of the H^+-accepting Ni-bound Cys597. (b) Excerpt of a sequence alignment of the large subunits from *Cn*MBH, *Ec*Hyd1, *Cn*RH, *Pf*SH1 and *Dv*MF hydrogenase. Two of the four cysteines coordinating the [NiFe] site are highlighted in yellow (ruler positions 82/85), conserved residues are highlighted in red, residues with similar features are framed in blue boxes, secondary structural elements (derived from PDB:3RGW (**https://www.rcsb.org/structure/3RGW**))[25] are shown on top of the alignment. *Cn*MBH carries an additional cysteine (Cys81, ruler position 88), which is also highlighted in yellow. The complete alignment is shown in Fig. S4 (ESI†). (c) [NiFe] active site structure of H_2-reduced *Cn*MBH characterized by a bimodal conformation of Cys81.[25] The thiolate group in conformation A (Cys81$_A$, 80% occupation) is located at a H-bond distance (dashed cyan lines) from both Cys78 and the CO ligand.

exhibit significantly higher intensities than those observed for the Ni$_a$-L1/L2 intermediates of *Cn*RH (Fig. S3, ESI†) and *Dv*MF.[11,14] Based on all spectroscopic, computational and structural data for [NiFe]-hydrogenases reported so far,[4,5] a protonated Ni-binding cysteine (Cys597 for *Cn*MBH) was not expected for the Ni$_a$-C state. However, *Cn*MBH contains an additional cysteine residue (Cys81) close to the active site, which is not present in other extensively characterized [NiFe]-hydrogenases such as *Ec*Hyd1, *Cn*RH, *Dv*MF hydrogenase and the soluble hydrogenase-1 from *Pyrococcus furiosus* (*Pf*SH1) (Fig. 3b, c and Fig. S4, ESI†). From the web database HydDB for hydrogenase classification,[24] we retrieved more than 200 sequences of [NiFe]-hydrogenase large subunits of the subgroup 1d (O_2-tolerant H_2-uptake [NiFe]-hydrogenases, ESI†) to which *Cn*MBH and *Ec*Hyd1 belong.

At the position corresponding to Cys81 of *Cn*MBH, polar amino acid residues are found in about 70% of the sequences and cysteine is the second most frequent amino acid (Fig. S5, ESI†). The crystal structure of *Cn*MBH shows that Cys81 is located in a water-filled pocket near the NiFe site and may be part of a proton transfer pathway.[16] Previous electrochemical studies have shown that replacing Cys81 in *Cn*MBH results in higher Michaelis constants (K_M) for H_2,[26] suggesting that this residue modulates the substrate affinity in *Cn*MBH. Cys81 adopts a predominant (*ca.* 80%, Cys81$_A$) conformation in the structure of H_2-reduced *Cn*MBH,[25] in which its thiolate group is in H-bonding distance to both the bridging Cys78 sulfur atom (3.4 Å) and the CO ligand (3.3 Å) (Fig. 3c). The active site geometry indicates that the sulfur atom of Cys78 is the main acceptor, since the proposed H-bond might adopt the preferred angle of almost 180°.[27] Importantly, this H-bond may cause a more polarized S–H bond of Cys81, resulting in higher absorption coefficients for the observed ν_{SH} bands. To test this hypothesis, we analysed an MBH variant in which Cys81 had been exchanged for the isosteric serine residue.[26] This should lead to an exchange of the thiolate for a hydroxy side group, and should facilitate the spectroscopic assignment without optimally altering the catalytic activity. In fact, the purified *Cn*MBH^{Cys81Ser} variant retained H_2 oxidation activity with a specific activity of 129.2 ± 9.6 U mg^{-1}, which is *ca.* 92% of the activity of native *Cn*MBH,[28] and is consistent with previous studies.[26,29] The IR spectroscopic data of the MBH^{Cys81Ser} variant in the as-isolated, H_2-reduced and re-oxidized forms, measured at 283 K, are shown in Fig. S6a–c (ESI†). After partial reduction of MBH^{Cys81Ser} with H_2 (trace *b* in Fig. S6a, ESI†), the sample was cooled to 95 K and then illuminated with LEDs at 460 nm (Fig. S6b, ESI†). The corresponding IR difference spectra (light-minus-dark, Ni$_a$-L-minus-Ni$_a$-C) of the MBH^{Cys81Ser} variant and that of native *Cn*MBH are depicted in Fig. S7 (ESI†), and a detailed analysis of the active site CO/CN^- absorptions is provided as part of the ESI.† Notably, the previously observed ν_{SH} bands of native *Cn*MBH are not present in the IR difference spectrum of the MBH^{Cys81Ser} variant. Therefore, we conclude that the observed S–H absorptions of native *Cn*MBH (Fig. 3a) originate from the protonated side chain of Cys81. In addition, the observed frequency shift for the ν_{SH} bands (2516 → 2523 cm^{-1}) during the Ni$_a$-C → Ni$_a$-L transformation suggests that the strength of the S–H bond of Cys81 is directly influenced by electronic/structural changes at the [NiFe] site. We propose that photolysis of the bridging hydride induces local changes in the H-bond network near the [NiFe] site, which causes the observed shift of the ν_{SH} for Cys81. The initial aim of this study was to analyse the protonation state of Cys597 in *Cn*MBH, and we expect Cys597 to be protonated in the case of the Ni$_a$-L1/2

intermediates. In fact, the spectral signals of the Ni_a-L species of *Cn*MBH are quite similar to those of *Cn*RH, in which the analogous Ni-bound cysteine resides in a protonated state (Fig. S3, ESI†).[14] In the case of native *Cn*MBH, the expected S–H absorption of Cys597 might be covered by the intense absorptions of Cys81, leaving only a remnant visible as an absorption at 2530 cm^{-1} (asterisk in Fig. 3a). Additionally, the simultaneous presence of two Ni_a-L sub-forms in *Cn*MBH implies a heterogeneous population of Cys597-S–H conformers, which reduces the probability of observing the corresponding S–H spectral features. The rather low enrichment of the Ni_a-C intermediate, especially in the $MBH^{Cys81Ser}$ variant (Fig. S6a, ESI†), might be another reason for the absence of clear signals from Cys597 protonation. Thus, future research will focus on the enrichment of Ni_a-C and Ni_a-L1/L2 species in both *Cn*MBH and variants devoid of Cys81 to specifically probe the spectral contribution of residues surrounding the [NiFe] site and the protonation state of Cys597. Our findings emphasize the necessity of a careful interpretation of the absorptions in the spectral region in which S–H signals occur. While the protonation of a Ni-bound cysteine (Cys597 in *Cn*MBH) seemed obvious given its role as a H^+ acceptor during catalysis,[14,30,31] the presented IR data shifted the focus to the more distant Cys81. Since several O_2-tolerant [NiFe]-hydrogenases of subgroup 1d contain a cysteine at this position (Fig. S5, ESI†), our data will support their biophysical investigation and the corresponding interpretation of the IR data. Furthermore, our observations are of general importance in (bio)catalysis as they might offer new insights for the investigation of biological and (semi-)synthetic systems (*e.g.*, nitrogenases,[32] Ni-containing rubredoxins,[33] de novo-designed hydrogenases[34]) which operate *via* transiently protonated thiolate functionalities.

This work was funded by the Deutsche Forschungsgemeinschaft (DFG, German Research Foundation) under Germany's Excellence Strategy – EXC 2008-390540038 ("Unifying Systems in Catalysis-UniSysCat"). O. L. and I. Z. are thankful for financial support from EU Horizon 2020/McGEA/Proposal ID 101183014 HORIZON-MSCA-2023-SE-01-01. The authors acknowledge Marius Horch and Yvonne Rippers for helpful discussions.

Data availability

The authors declare that the data supporting the findings of this study are available within the article and the ESI.†

Conflicts of interest

There are no conflicts to declare.

Notes and references

1 G. Caserta, S. Hartmann, C. Van Stappen, C. Karafoulidi-Retsou, C. Lorent, S. Yelin, M. Keck, J. Schoknecht, I. Sergueev, Y. Yoda, P. Hildebrandt, C. Limberg, S. DeBeer, I. Zebger, S. Frielingsdorf and O. Lenz, *Nat. Chem. Biol.*, 2023, **19**, 498–506.
2 J. Fritsch, O. Lenz and B. Friedrich, *Nat. Rev. Microbiol.*, 2013, **11**, 106–114.
3 S. T. Stripp, B. R. Duffus, V. Fourmond, C. Léger, S. Leimkühler, S. Hirota, Y. Hu, A. Jasniewski, H. Ogata and M. W. Ribbe, *Chem. Rev.*, 2022, **122**, 11900–11973.
4 P. A. Ash, R. Hidalgo and K. A. Vincent, *ACS Catal.*, 2017, **7**, 2471–2485.
5 W. Lubitz, H. Ogata, O. Rüdiger and E. Reijerse, *Chem. Rev.*, 2014, **114**, 4081–4148.
6 C. M. Silveira, L. Zuccarello, C. Barbosa, G. Caserta, I. Zebger, P. Hildebrandt and S. Todorovic, *Molecules*, 2021, **26**, 4852.
7 G. Caserta, L. Zuccarello, C. Barbosa, C. M. Silveira, E. Moe, S. Katz, P. Hildebrandt, I. Zebger and S. Todorovic, *Coord. Chem. Rev.*, 2022, **452**, 214287.
8 B. L. Greene, G. E. Vansuch, B. C. Chica, M. W. W. Adams and R. B. Dyer, *Acc. Chem. Res.*, 2017, **50**, 2718–2726.
9 S. T. Stripp, *ACS Catal.*, 2021, **11**, 7845–7862.
10 M. Senger, V. Eichmann, K. Laun, J. Duan, F. Wittkamp, G. Knör, U.-P. Apfel, T. Happe, M. Winkler, J. Heberle and S. T. Stripp, *J. Am. Chem. Soc.*, 2019, **141**, 17394–17403.
11 H. Tai, K. Nishikawa, Y. Higuchi, Z. Mao and S. Hirota, *Angew. Chem., Int. Ed.*, 2019, **58**, 13285–13290.
12 H. Tai, S. Hirota and S. T. Stripp, *Acc. Chem. Res.*, 2021, **54**, 232–241.
13 H. Tai, K. Nishikawa, S. Inoue, Y. Higuchi and S. Hirota, *J. Phys. Chem. B*, 2015, **119**, 13668–13674.
14 A. F. T. Waffo, C. Lorent, S. Katz, J. Schoknecht, O. Lenz, I. Zebger and G. Caserta, *J. Am. Chem. Soc.*, 2023, **145**, 13674–13685.
15 P. A. Ash, S. E. T. Kendall-Price, R. M. Evans, S. B. Carr, A. R. Brasnett, S. Morra, J. S. Rowbotham, R. Hidalgo, A. J. Healy, G. Cinque, M. D. Frogley, F. A. Armstrong and K. A. Vincent, *Chem. Sci.*, 2021, **12**, 12959–12970.
16 S. Frielingsdorf, J. Fritsch, A. Schmidt, M. Hammer, J. Löwenstein, E. Siebert, V. Pelmenschikov, T. Jaenicke, J. Kalms, Y. Rippers, F. Lendzian, I. Zebger, C. Teutloff, M. Kaupp, R. Bittl, P. Hildebrandt, B. Friedrich, O. Lenz and P. Scheerer, *Nat. Chem. Biol.*, 2014, **10**, 378–385.
17 G. Caserta, V. Pelmenschikov, C. Lorent, A. F. Tadjoung Waffo, S. Katz, L. Lauterbach, J. Schoknecht, H. Wang, Y. Yoda, K. Tamasaku, M. Kaupp, P. Hildebrandt, O. Lenz, S. P. Cramer and I. Zebger, *Chem. Sci.*, 2021, **12**, 2189–2197.
18 J. A. Birrell, V. Pelmenschikov, N. Mishra, H. Wang, Y. Yoda, K. Tamasaku, T. B. Rauchfuss, S. P. Cramer, W. Lubitz and S. DeBeer, *J. Am. Chem. Soc.*, 2020, **142**, 222–232.
19 C. Karafoulidi-Retsou, C. Lorent, S. Katz, Y. Rippers, H. Matsuura, Y. Higuchi, I. Zebger and M. Horch, *Angew. Chem., Int. Ed.*, 2024, e202409065.
20 R. Hidalgo, P. A. Ash, A. J. Healy and K. A. Vincent, *Angew. Chem., Int. Ed.*, 2015, **54**, 7110–7113.
21 H. Tai, K. Nishikawa, M. Suzuki, Y. Higuchi and S. Hirota, *Angew. Chem., Int. Ed.*, 2014, **53**, 13817–13820.
22 B. L. Greene, G. E. Vansuch, C.-H. Wu, M. W. W. Adams and R. B. Dyer, *J. Am. Chem. Soc.*, 2016, **138**, 13013–13021.
23 V. A. Lorenz-Fonfria, *Chem. Rev.*, 2020, **120**, 3466–3576.
24 D. Søndergaard, C. N. S. Pedersen and C. Greening, *Sci. Rep.*, 2016, **6**, 34212.
25 J. Fritsch, P. Scheerer, S. Frielingsdorf, S. Kroschinsky, B. Friedrich, O. Lenz and C. M. T. Spahn, *Nature*, 2011, **479**, 249–252.
26 M. Ludwig, J. A. Cracknell, K. A. Vincent, F. A. Armstrong and O. Lenz, *J. Biol. Chem.*, 2009, **284**, 465–477.
27 D. Herschlag and M. M. Pinney, *Biochemistry*, 2018, **57**, 3338–3352.
28 J. Fritsch, S. Löscher, O. Sanganas, E. Siebert, I. Zebger, M. Stein, M. Ludwig, A. L. De Lacey, H. Dau, B. Friedrich, O. Lenz and M. Haumann, *Biochemistry*, 2011, **50**, 5858–5869.
29 M. Saggu, M. Ludwig, B. Friedrich, P. Hildebrandt, R. Bittl, F. Lendzian, O. Lenz and I. Zebger, *ChemPhysChem*, 2010, **11**, 1215–1224.
30 R. M. Evans, N. Krahn, J. Weiss, K. A. Vincent, D. Söll and F. A. Armstrong, *J. Am. Chem. Soc.*, 2024, **146**, 16971–16976.
31 A. Sirohiwal, A. P. Gamiz-Hernandez and V. R. I. Kaila, *J. Am. Chem. Soc.*, 2024, **146**, 18019–18031.
32 K. Sengupta, J. P. Joyce, L. Decamps, L. Kang, R. Bjornsson, O. Rüdiger and S. DeBeer, *J. Am. Chem. Soc.*, 2025, **147**, 2099–2114.
33 J. W. Slater, S. C. Marguet, M. E. Gray, H. A. Monaco, M. Sotomayor and H. S. Shafaat, *ACS Catal.*, 2019, **9**, 8928–8942.
34 S. Malayam Parambath, D. Prakash, W. Swetman, A. Surakanti and S. Chakraborty, *Chem. Commun.*, 2023, **59**, 13325–13328.